JOURNAL OF AIRCRAFT
Vol. 46, No. 5, September–October 2009

# Multistep Results in ICECREMO2

P. Verdin*
*Cranfield University, Cranfield, Bedfordshire MK43 0AL, United Kingdom*
J. P. F. Charpin†
*University of Limerick, Limerick, Ireland*
and
C. P. Thompson‡
*Cranfield University, Cranfield, Bedfordshire MK43 0AL, United Kingdom*

DOI: 10.2514/1.41451

**Multistep versions of the aircraft icing code ICECREMO2 are investigated. Several multistep algorithms are presented and tested on a NACA0012 wing in rime and glaze ice conditions. The resulting ice layers are compared with experimental results and the efficiency of each algorithm is discussed. The step-by-step algorithm with an ice height criterion provided the most time-efficient solution in glaze ice conditions.**

## Nomenclature

| | | |
|---|---|---|
| $b$ | = | ice layer thickness, m |
| $c$ | = | chord length, m |
| $c_a$ | = | specific heat capacity of air, J kg$^{-1}$K$^{-1}$ |
| $c_i$ | = | specific heat capacity of ice, J kg$^{-1}$K$^{-1}$ |
| $d_d$ | = | droplet diameter, m |
| $E$ | = | heat balance coefficient, K m$^{-1}$ |
| $e_0$ | = | vapour pressure constant, Pa K$^{-1}$ |
| $e_*$ | = | unit vector in the $x$, $y$, and $z$ directions, ND |
| $F$ | = | heat balance coefficients, m$^{-1}$ |
| $g$ | = | acceleration due to gravity, m s$^{-2}$ |
| $H$ | = | heat transfer coefficient at the ice air interface, W m$^{-2}$ K$^{-1}$ |
| $h$ | = | water layer thickness, m |
| $L_f$ | = | latent heat of fusion, J kg$^{-1}$ |
| ND | = | nondimensional |
| $n_{\text{step}}$ | = | number of multi time steps |
| $Q_x$ | = | $x$ component of the water flux, m$^2$ s$^{-1}$ |
| $Q_y$ | = | $y$ component of the water flux, m$^2$ s$^{-1}$ |
| $r$ | = | local recovery factor, ND |
| $T$ | = | temperature in the ice layer, K |
| $T_f$ | = | freezing temperature, K |
| $T_s$ | = | substrate temperature, K |
| $T_\infty$ | = | freestream temperature, K |
| $t$ | = | time, s |
| $t_{\text{exp}}$ | = | exposure time, s |
| $V_\infty$ | = | freestream velocity, m s$^{-1}$ |
| $X$ | = | ice height to chord length ratio, ND |
| x,y | = | Cartesian coordinates, m |
| $\beta$ | = | collection efficiency, ND |
| $\theta$ | = | temperature in the water layer, K |
| $\kappa_i$ | = | thermal conductivity of the ice, W m$^{-1}$ K$^{-1}$ |
| $\kappa_w$ | = | thermal conductivity of the water, W m$^{-1}$ K$^{-1}$ |
| $\mu$ | = | dynamic viscosity, kg m$^{-1}$ s$^{-1}$ |
| $\rho$ | = | cloud liquid water content of air, kg m$^{-3}$ |
| $\rho_i$ | = | density of the ice, kg m$^{-3}$ |
| $\rho_w$ | = | density of the water, kg m$^{-3}$ |
| $\tau_x$ | = | $x$ component of the shear stress, Pa |
| $\tau_y$ | = | $y$ component of the shear stress, Pa |
| $\chi$ | = | evaporation coefficient, m s$^{-1}$ |

Received 8 October 2008; revision received 2 April 2009; accepted for publication 2 April 2009. 

*Lecturer/Research Fellow, Applied Mathematics and Computing, School of Engineering.
†Senior Research Fellow, Mathematics Applications Consortium for Science and Industry, Department of Mathematics and Statistics.
‡Professor, Applied Mathematics and Computing, School of Engineering.

## I. Introduction

ICE accretion is a major concern for aircraft manufacturers. Over the years, numerous incidents or accidents have occurred because of ice growing on key parts of the plane [1,2]. To limit the consequences of ice accretion and guarantee safety, manufacturers are required to test all aircraft for icing and equip them with adequate anti-icing or deicing systems. Computer codes are used to assist manufacturers with design and certification work required by the aircraft industry. The first aircraft icing codes to appear were NASA Lewis Ice Accretion Prediction Code (LEWICE) developed by NASA in the United States, Trajectory and Ice Accretion Code (TRAJICE) in the United Kingdom, engineered by what has now become QinetiQ, and Office National d'Etudes et de Recherches Aérospatiales (ONERA) in France [3–5]. Italian and Canadian codes, among others, appeared later [6–9]. At first, all the codes were based on the work of Messinger [10]. This model, developed in the fifties, proved quite successful. However, weaknesses have been found [11]: the Messinger model overestimates the ice growth and the error increases with the ambient temperature. With this original model, the ice formation is not affected by the existing ice layer, the ice growth rate is constant throughout the simulation and the fluid flow depends on the size of the mesh chosen for the simulation. Some of these difficulties were partially addressed by the various development teams. All these problems could only be solved simultaneously with a new model detailed in [12,13]. This improved model is used in the icing code called ICECREMO2, developed by a number of companies in the United Kingdom (see acknowledgments).

Icing occurs in cold and wet conditions. In this situation, the cloud droplets can be in a liquid state, although their temperature is below freezing. When droplets hit the aircraft wing, they turn to ice almost instantaneously and form what is known as rime ice. In mild conditions and once the rime ice layer is thick enough, part of the impinging droplet may remain liquid and form a thin film that runs back over the ice layer [14]. The ice formed in these conditions is known as glaze ice. Icing codes reflect these two different possibilities and flow parameters necessary for each phase must be calculated.

When simulating an ice shape, physical parameters influencing the accretion (shear stress, heat transfer coefficient, and water droplet trajectories) are first evaluated on the clean uniced airfoil at the beginning of the calculation and are held constant during the entire

computation. This procedure is known as a single-step calculation. The values calculated on an ice-clean body become less accurate when the ice layer thickens and exposure time to icing increases: for large enough shapes, the presence of ice influences the airflow, leading to significant changes in key icing parameters. To obtain more accurate results, the flowfield around the body should be recomputed periodically during the simulation and the values of important icing parameters should be updated. This procedure, known as multistepping, is used in several Messinger-based codes. The objective of this work is to investigate multistep algorithms using the ICECREMO2 icing code based on the icing model developed in [12,13].

In the following, the structure of a multistep icing code is discussed in Sec. II.A, and possible algorithms are presented. The icing model used in ICECREMO2 is then briefly described in Sec. II.B. Governing equations are introduced for rime and glaze ice growth and parameters likely to vary significantly during an icing calculation are pointed out. Numerical results are then presented for a NACA0012 airfoil in rime ice conditions in Sec. III.A and in glaze ice conditions in Sec. III.B. When possible, the numerical solutions calculated with ICECREMO2 are compared with experimental results and with simulations performed using alternative icing codes.

## II. Models

Ice shapes are simulated using standard methods. Classical icing algorithms are presented in Sec. II.A. A key feature in these algorithms is the heat balance governing the ice growth. This will be detailed in Sec. II.B.

### A. Icing Code Structure

Icing codes are generally split into four parts [15,16]. The flow around the body is determined first, using computational fluid dynamics. Water droplet trajectories are then simulated to evaluate the collection efficiency. This parameter, reflecting the quantity of liquid impinging on the wing surface, is calculated during the third stage, together with the heat transfer coefficient. Finally, a thermal analysis is performed to determine the ice growth.

The structure of a typical ice prediction code may be summarized as:

1) Solve for the airflow around the body.

2) Study the droplet trajectories.

3) Calculate the collection efficiency and other physical parameters influencing the ice accretion.

4) Perform a thermal analysis to determine the ice accretion.

This algorithm is known as a single-step method: the physical parameters required to perform the thermal analysis are calculated at the start of the simulation on the clean uniced airfoil and they remain constant during the entire calculation. Many of the parameters will vary as the ice grows, therefore multistep algorithms have been developed to allow for variations. For example, the step-by-step and predictor–corrector algorithms.

#### 1. *Step-by-Step Algorithm*

The step-by-step algorithm is the most widely used procedure [7,17,18]. In this method, the constant value of parameters is replaced by a piecewise constant function of time, see Fig. 1. The four parts of the one-step algorithm are repeated as many times as necessary. A criterion defining the start of a new cycle is specified and the corresponding ice growth rates are determined. The initial geometry is then adjusted to account for the accreted ice and a new flowfield calculation is performed around the iced geometry. This procedure is iterated until the specified total icing exposure time is reached. The algorithm relative to this approach is summarized on Fig. 2.

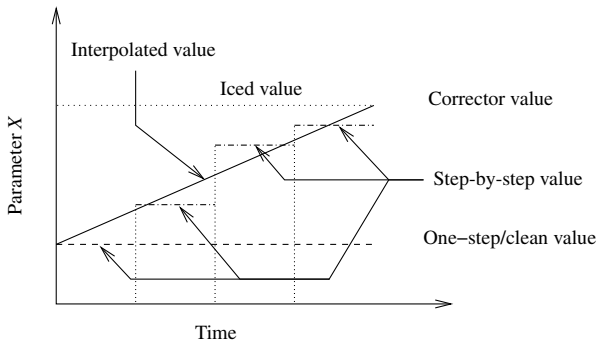


**Fig. 1 Variation of parameter $X$ during a multistep icing algorithm.**

A step-by-step calculation is potentially rather time consuming due to the numerous flow calculations; the criterion triggering the start of a new cycle and a new flow calculation need to be defined with care. The importance of a suitable number of time steps has been outlined in [5]. Most commonly, the total icing exposure time is divided into a given number of equal time increments. The user may choose the duration of time steps with an educated guess. Alternatively, some guidelines are available. According to Wright [3], the maximum accumulated thickness of ice in any step should not be greater than 1% of the wing chord length. The number of steps denoted $n_{\text{step}}$ may be estimated using the expression [19]:

$$n_{\text{step}} = \frac{1}{cX}\frac{\rho V_\infty t_{\text{exp}}}{\rho_i} \tag{1}$$

where the notation is defined in the Nomenclature section. The term $\rho V \infty t_{\text{exp}}/\rho_i$ represents the maximum amount of ice that could be growing over the impact surface during the exposure time $t_{\text{exp}}$ and $cX$ corresponds to the maximum thickness of ice allowed to grow during a multistep, expressed as a function of the chord length. For very small geometries, this may lead to a prohibitive number of time steps [20] and other options should also be investigated. A time based criterion may not be the most appropriate method when glaze ice is growing. In this situation, only part of the impinging water freezes when it reaches the substrate. Water runs back over the existing ice surface and calculating the growth of an ice layer is less straightforward. Time steps of constant duration may therefore not reflect the ice growth rate and the airflow could be recalculated too early or sometimes too late. A criterion based on the ice height may therefore be more effective. A new flow calculation is started when the maximum ice height growing during a time step reaches a value chosen by the user. The time steps would be longer when ice grows slowly and shorter for higher ice growth rates and this should reduce the number of time steps [21].

Even with a careful choice of triggering criteria, step-by-step algorithms can remain very time consuming due to the numerous flow calculations required. A potentially more time efficient multistep solution is the predictor–corrector algorithm.

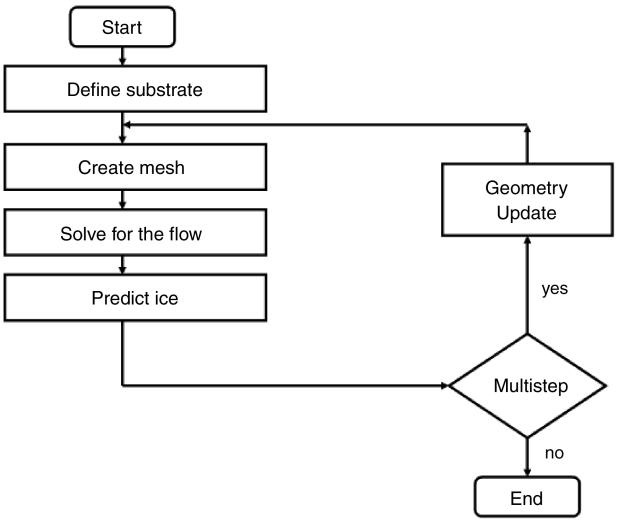


**Fig. 2 Multistep icing algorithm.**

*2. Predictor–Corrector Algorithm*

The predictor–corrector approach [8,17,22] is an alternative to the step-by-step calculation. This algorithm aims to simulate the continuous variation of the physical parameters using interpolations, see Fig. 1.

This procedure may be summarized as:

1) Determine the flow and icing parameters on the clean body.

2) Perform an ice accretion calculation using the constant "clean" value in a single-step procedure.

3) Determine the flow around the iced shape and recalculate the parameters on the iced body.

4) Perform a new ice calculation using time-dependent values for the physical parameters determined via an interpolation between the clean and the "iced" value.

If convergence is not be achieved at the end of step 4, a few extra iterations are necessary:

5) Determine the flow around the new iced shape and recalculate the parameters on the iced body,

6) Perform a new ice calculation using time-dependent values for the physical parameters determined via an interpolation between the clean and the iced value calculated in step 5.

Repeat steps 5 and 6 until convergence is reached, that is, until repeating steps 5 and 6 one more time does not change the ice profile significantly.

If only one iteration is necessary to reach convergence, the predictor–corrector procedure limits the number of new flowfield calculations in comparison with the step-by-step approach. In the latter, several flow evaluations are generally required whereas in a predictor–corrector approach, only two are necessary to obtain the estimated ice shape.

The multistep algorithms discussed in this section must be coupled with a thermal analysis leading to the ice growth algorithm. The models used in ICECREMO2 will now be briefly presented. This analysis will also determine what parameters should be updated when using a multistep calculation.

### B. Icing Models

As already mentioned, ice grows in two phases: rime ice appears first and then glaze ice. Each phase requires a specific model, they will now be detailed.

*1. Rime Ice Growth*

Rime ice grows in cold conditions. In this situation, the impinging droplets freeze almost instantaneously when they reach the surface. The ice growth rate may then be calculated using a mass balance:

$$\frac{\partial b}{\partial t} = \frac{\beta \rho V_\infty}{\rho_i} \tag{2}$$

where $b$ is the thickness of the ice layer (all parameters are defined in the Nomenclature section). The "catch" or collection efficiency, $\beta$, is the ratio of the mass flux hitting the surface to the mass flux that would hit if water droplets had straight line trajectories. It must be computed using the results of the flow calculation and is therefore likely to vary significantly when the ice layer increases. This parameter should be updated when using multistep methods. This model is similar in all icing codes.

*2. Glaze Ice Growth*

When the ice layer is thick enough, some of the impinging droplets may remain liquid and a water layer forms at the top of the ice accretion. This layer will remain extremely thin but it is key to accurate simulations. The mass balance (2) is then replaced by

$$\rho_i \frac{\partial b}{\partial t} + \rho_w \left( \frac{\partial h}{\partial t} + \nabla \cdot Q \right) = \beta \rho V_\infty \tag{3}$$

where the flux $Q$ is defined by

$$Q_x = -\frac{\rho_w g h^3}{3\mu} g \cdot e_x + \frac{\tau_x h^2}{2\mu} \tag{4}$$

$$Q_y = -\frac{\rho_w g h^3}{3\mu} g \cdot e_y + \frac{\tau_y h^2}{2\mu} \tag{5}$$

and $h$ is the thickness of the water layer. The mass balance (3) accounts for the evolution of the ice layer thickness and the movement of the water layer through the flux. The shear stress $(\tau_x, \tau_y)$ is highly dependent on the flow and should be updated during multistep calculations. The derivation of these equations is given in [23]. In the present model they are derived on a flat surface, but they may be extended to arbitrary shaped surfaces in [13], and examples for ice growth on cables and airfoils are given in [24].

Equation (3) is not enough to determine both the ice growth rate, $\partial b/\partial t$, and the water growth rate, $\partial h/\partial t$. It must be coupled with the Stefan condition:

$$\rho_i L_f \frac{\partial b}{\partial t} = \kappa_i \frac{\partial T}{\partial z} - \kappa_w \frac{\partial \theta}{\partial z} \tag{6}$$

where the temperatures, $T$ and $\theta$ in the ice and water layers, are governed by the two equations

$$\frac{\partial^2 T}{\partial z^2} \approx 0, \qquad \frac{\partial^2 \theta}{\partial z^2} \approx 0 \tag{7}$$

The conditions governing the validity of these approximations may be found in [23]. The corresponding boundary conditions are

$$T(0) = T_s, \qquad T(b) = T_f, \qquad \theta(b) = T_f$$

$$\left.\frac{\partial \theta}{\partial z}\right|_{b+h} = E - F\theta_{z=b+h}$$

where $E$ and $F$ reflect the physics at the top of the ice layer including convective heat transfer, water evaporation, kinetic energy, and aerodynamical heating:

$$E = \frac{\frac{\beta \rho V_\infty^3}{2} + \frac{r H V_\infty^2}{2 c_a} + \beta \rho V_\infty c_w + H T_\infty + \chi e_0 T_\infty}{\kappa_w}$$

$$F = \frac{\beta \rho V_\infty c_w + H + \chi e_0}{\kappa_w}$$

and all the notation is defined in the nomenclature. A full description of the terms may be found in [24]. All the parameters involved in $E$ and $F$ are constant except for the collection efficiency, $\beta$, and the heat transfer coefficient, $H$ (this parameter depends on the velocity at the edge of the boundary layer above the ice [14]). These two coefficients must be updated when using a multistep algorithm.

A straightforward integration of (6) leads to the updated Stefan condition:

$$\rho_i L_f \frac{\partial b}{\partial t} = \kappa_i \frac{T_f - T_s}{b} - \kappa_w \frac{E - F T_f}{1 + F h} \tag{8}$$

and the model is complete. While the rime ice model is used in all icing codes, the present glaze ice model is specific to ICECREMO2: the ice growth rate now varies with time, the water layer evolution is independent of the mesh size [11], and experimental comparisons show that the model accurately predicts the switch between rime and glaze ice [12]. The ICECREMO2 model reduces to the Messinger glaze ice model when conduction in the layers is neglected [11].

Ice shapes will now be calculated with the algorithms presented in this section. The collection efficiency, the shear stress, and the heat transfer coefficient will be updated at the end of each time step.

## III. Numerical Results

The multistep algorithms will now be tested on a NACA0012 for two cases. The conditions used for these two configurations may be found in Table 1. Since the geometries and simulation times are quite unrelated, the results are presented separately for rime ice and glaze ice cases.

**Table 1 Airflow and icing conditions applied to a NACA0012 wing [25,26]**

| Ice type | $T_\infty$, °C | $V_\infty$, m.s$^{-1}$ | $d_d$, $\mu$m | $t_{\text{exp}}$, min | $\alpha$, ° | chord, m | $\rho$, kg/m$^3$ | $\rho_i$, kg/m$^3$ |
|---|---|---|---|---|---|---|---|---|
| Rime | −26 | 67 | 20 | 6 | 4 | 0.533 | 0.001 | 880 |
| Glaze | −7 | 67 | 25 | 20 | 3 | 0.914 | 0.001 | 910 |

The flow around the airfoil was calculated using the FLUENT package. Air was modeled as an ideal gas and the one equation Spalart-Allmaras model of turbulence [27] was chosen as it has proved efficient for external flow calculations involving icing [28]. The mesh was generated automatically using GAMBIT. The procedure was tested on the clean geometry and mesh parameters were chosen to guarantee a good agreement between the simulated and the experimental results. The clean geometry parameters are used for all the mesh generations throughout the simulation.

### A. Rime Ice

Rime ice is generally easier to simulate and the algorithms are tested on this slightly less problematic configuration first. Results are presented for the step-by-step algorithm with the two flow triggering criteria presented in Sec. II.B and for the predictor–corrector algorithm. In all three cases, the ambient temperature is $T_\infty = -26$°C, and supercooled droplets of diameter $d = 20$ $\mu$m collide with a NACA0012 wing of chord length $c = 0.533$ m for 6 min.

#### 1. *Step-by-Step Time Criterion*

Figure 3 shows the experimental ice shape as measured by Shin and Bond [25] and ice shapes simulated using the step-by-step method with the time criterion. In all cases, for single-step and multistep calculations, the calculations significantly overestimate the ice layer at the leading edge of the wing, and slightly underestimate the accretion further downstream. Using the multistep algorithm reduces the excess of ice away from the leading edge stagnation line. The number of steps during the simulation is increased progressively and the ice shape does not vary significantly from 5 flow calculations. This means one update every 72 s. Using Eq. (1), this number corresponds to 1% of the chord length. This is consistent with the results obtained in [19].

#### 2. *Step-by-Step Ice Height Criterion*

The simulations are now carried out with the step-by step algorithm using the ice height criterion. The height at which a new flow calculation must be started is defined as a proportion of the chord length. This value is decreased progressively to study convergence. As may be seen on Fig. 4, convergence is reached for an ice height criterion, $b_{\max} = 0.8\%c$, which corresponds to five flow calculations. The ice layer is very similar to the shape obtained with the time criterion: the accretion is overestimated close to the stagnation line and slightly underestimated further downstream. It appears that for rime ice, the criterion used does not make a significant difference.

#### 3. *Predictor–Corrector*

The ice accretion is now estimated using the predictor–corrector method. Convergence is reached from the first correction and there is no need to iterate the process further. Figure 5 compares the experimental ice accretion to the shapes estimated using a step-by-step algorithm and the predictor–corrector algorithm. The two criteria used for the step-by-step analysis lead to virtually the same curves and only one is represented here. The predictor–corrector shape differs only slightly from the step-by-step layer. The step-by-step and predictor–corrector algorithms lead to similar quality ice height estimations but the predictor–corrector algorithm only required two flow calculations against five for the step-by-step methods. Since flow calculations are so time consuming, the predictor–corrector algorithm should be favored in rime ice conditions. This was also the conclusion reached in [8] when using the Messinger model.

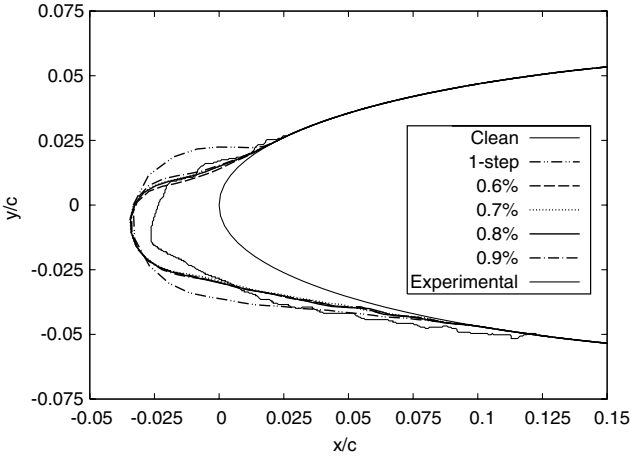


**Fig. 4 Rime ice step-by-step calculation with ice height criterion. $T_\infty = -26$°C, $t_{\text{exp}} = 6$ min.**

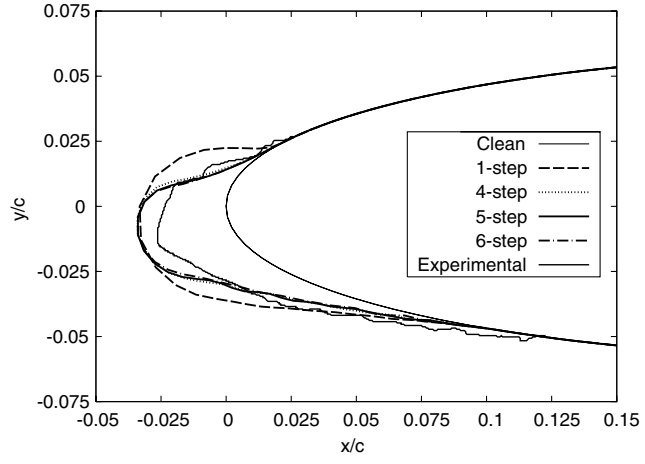


**Fig. 3 Rime ice step-by-step calculation with time criterion. $T_\infty = -26$°C, $t_{\text{exp}} = 6$ min.**

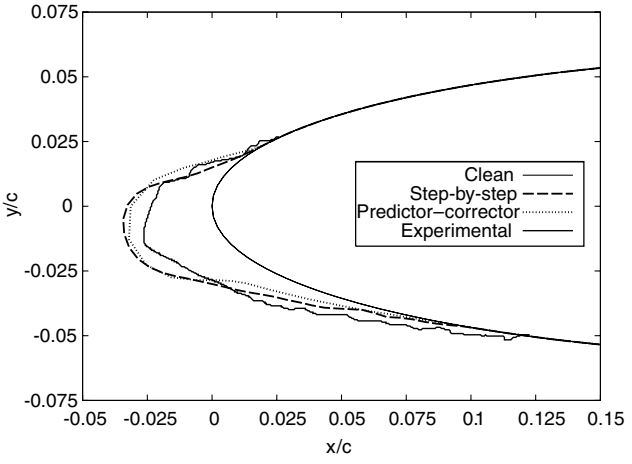


**Fig. 5 Step-by-step versus predictor–corrector. $T_\infty = -26$°C, $t_{\text{exp}} = 6$ min.**

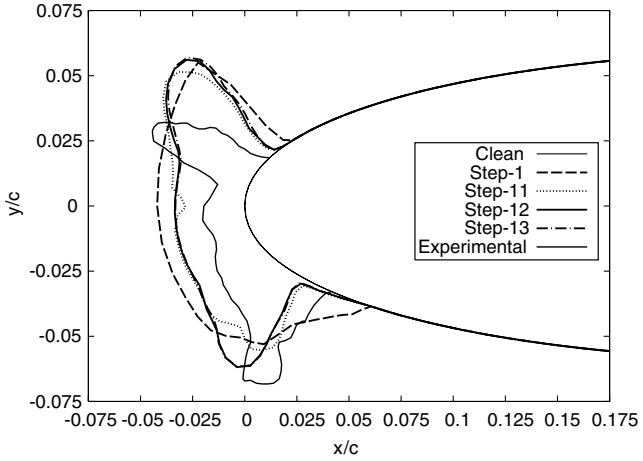


**Fig. 6 Step-by-step calculation based on the time criterion. $T_\infty = -7°C, t_{exp} = 20$ min.**

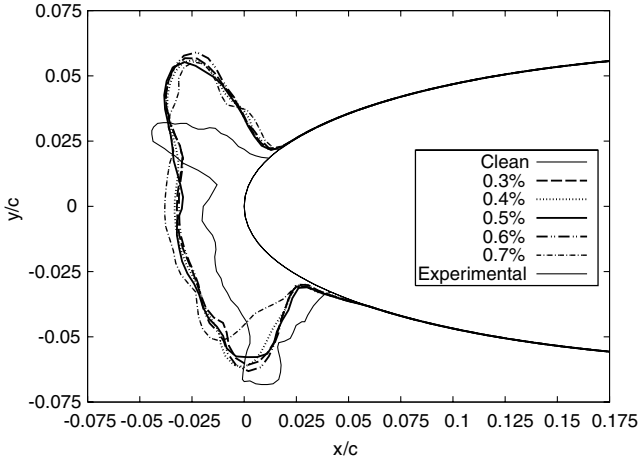


**Fig. 7 Step-by-step calculation, ice height criterion. $T_\infty = -7°C$, $t_{exp} = 20$ min.**

### B. Glaze Ice

Because of the presence of the thin water layer at the top of the ice layer, glaze ice is much more difficult to simulate. Results will now be presented for the same three algorithms for the ambient temperature $T_\infty = -7°C$ and supercooled droplets of diameter $d = 25\ \mu$m impacting on a NACA0012 wing of chord length $c = 0.914$ m for 20 min.

#### 1. *Step-by-Step Time Criterion*

Figure 6 shows the experimental results and the ice shape simulated for various numbers of steps. As in the rime ice situation, the thickness of the accreted layer is overestimated. However, the two horns typical of glaze ice growth appear very clearly, though not quite in the right location. These difficulties are due to the complexity of the ice shape that significantly disturbs the flow and make flow results particularly difficult to calculate accurately. This is also related to the nature of the model used to calculate the ice shape. In this model the ice height and ice growth rate is defined orthogonally to the wing surface. This assumption is obviously wrong close to the horns.

As may be seen in Fig. 6, convergence is not as obvious as it was for the rime ice situation. However, the shape almost stabilizes for 12 flow calculations and then oscillates around this shape. The variation is due principally to the automatic generation of grid that becomes more difficult to control for a complex shape. Using Eq. (1), this leads to $X = 0.8\%$ of the chord length. This value is consistent with the recommendations of [3], where a value lower than 1% is suggested, and with the results obtained with rime ice in the previous section.

#### 2. *Step-by-Step Ice Height Criterion*

The ice layer is now simulated using the ice height criterion. Here again, the height that triggers a new flow calculation is expressed as a percentage of the chord length and this value is decreased until convergence is achieved. The shape stops changing significantly for $b_{max} \leq 0.6\%c$ as shown on Fig. 7. The ice shape has the same characteristics as the layer calculated with the time criterion. The two horns are slightly larger and the accretion is a little bit thinner close to the leading edge. The two shapes may be considered of equal quality.

Using a maximum ice growth of $b_{max} = 0.6\%c$ per step requires 10 flow calculations, which is two less than the time criterion, corresponding to a 17% reduction in time. Figure 8 compares the time at which the flow is recalculated for both criteria. By definition, the time criterion calculations occur at regular time intervals. The situation is quite different with the ice height criterion: at first, the multisteps last longer, around 2 min and 30 s against 1 min and 40 s for the time criterion. The duration of multisteps then reduces to a value slightly below 2 min. Flow recalculations are clearly related to the glaze ice features as may be seen on Fig. 9. The late stage of the ice growth is the most demanding and requires the shortest multisteps. When the ice height criterion is used, the length of the multisteps is adapted automatically and this has no influence on the early stages of the ice growth. When the time criterion is used, the shortest multistep value must be used throughout the calculation particularly at the start where longer steps could be allowed. In the end, the time criterion requires more multisteps to achieve an equivalent level of accuracy. For this example, the ice height criterion is clearly more efficient and should be preferred to the standard time criterion.

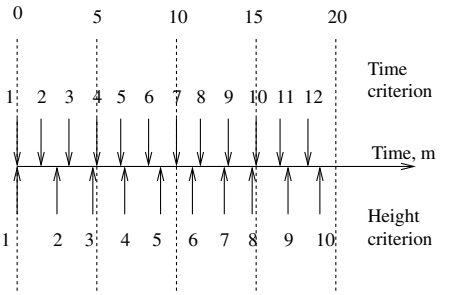


**Fig. 8 Time when a flow calculation is triggered.**

#### 3. *Predictor–Corrector*

Finally, the ice shape is calculated using the predictor–corrector method. Five corrections were necessary to reach a converged shape, meaning six flow calculations in total. The final shape may be seen on

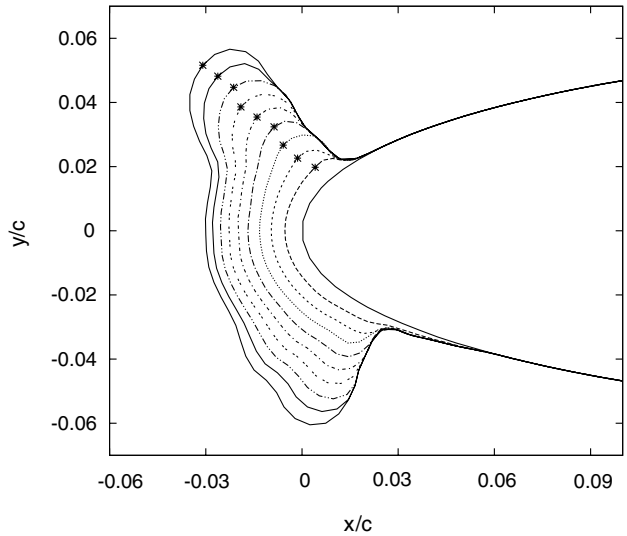


**Fig. 9 Critical points determining when a new flow calculation is triggered.**

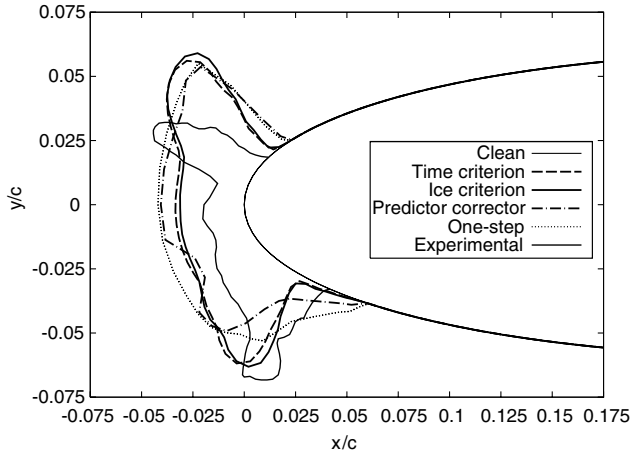


**Fig. 10 Criteria comparison. $T_\infty = -7°\mathrm{C}, t_{\mathrm{exp}} = 20$ min.**

Fig. 10 together with the experimental results and the shape calculated using the step-by-step method. The accretion estimated with the predictor–corrector algorithm is less accurate than the results obtained using a step-by-step approach. The horns are hardly visible and the entire shape is shifted towards the upper part of the wing. Compared with the step-by-step algorithm, the predictor–corrector method requires half the number of flow calculations, and so computation time is divided by two, but the computed ice layer is significantly less accurate.

These results are consistent with the conclusions of [29]: the predictor–corrector algorithm works best for rime ice conditions. In this situation, the ice growth depends solely on the collection efficiency, a parameter that does not vary hugely when ice accretes. The situation is quite different with glaze ice where the heat transfer coefficient and shear stress play a major role in the ice growth rate. In addition, the predictor–corrector approach is more sensitive to the quality of the flow solution than the step-by-step method. A low quality solution would only affect the ice growth during a fraction of the calculation in the step-by-step environment while it would affect the entire calculation with lasting effects with the predictor–corrector algorithm. A step-by-step approach should therefore be favored in glaze ice conditions.

#### 4. *Comparison with Other Codes*

The results are now compared with shapes calculated using standard multistep versions of the icing codes LEWICE [3,30], TRAJICE [5,14], and ONERA [31,32], see Fig. 11. Since codes evolve constantly and are always being improved, the shapes obtained with these codes may be different if they were simulated again today. However, for lack of more recent data, the results of the North Atlantic Treaty Organization (NATO) Research and Technology Ogranization (RTO) exercise held in December 2000 [26] are used as references.

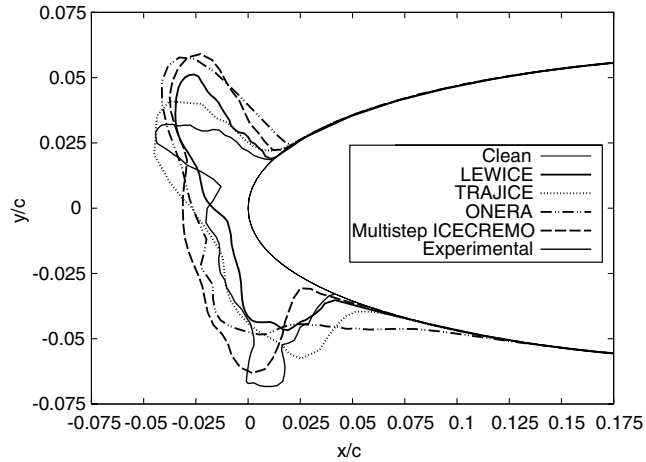


**Fig. 11 Step-by-step simulation using the ice height criterion. Comparison with other icing codes $T_\infty = -7°\mathrm{C}, t_{\mathrm{exp}} = 20$ min.**

As already mentioned, the glaze ice shape studied in this section is very difficult to reproduce numerically. As shown in Fig. 11, all codes overestimate the ice layer, and none of them matches the experimental shape perfectly. All four codes give similar results in the upper horn region with TRAJICE and LEWICE describing the shape more accurately. The lower horn region is best matched by ICECREMO2 and TRAJICE. Overall, the step-by-step version of ICECREMO2 leads to one of the best approximations for the ice shape and the algorithm used here is an improvement from the codes used in the NATO RTO study. The main difference between the codes is the icing model. The criteria used to trigger a new flow calculation are nearly similar. Although it was not possible to compare the present results with ICECREMO2 simulations calculated with the Messinger model, the icing model appears as a key element to the improvement of the ice shape. The carefully chosen criterion triggering the flow recalculation is key in reducing the time required to reach the best possible shape, but the result is still different from the correct shape.

## IV. Conclusion

Two multistep versions of the aircraft icing code ICECREMO2 were presented:

1) A step-by-step method with a flow calculation triggered by a time based criterion or an ice height based criterion.

2) A predictor–corrector approach.

In rime ice conditions, the predictor–corrector algorithm was the most efficient with only two flow calculations required to reach a good quality converged shape. In glaze ice conditions, the step-by-step method using the ice height based triggering criterion proved the most effective with a 17% reduction in the time required to calculate a converged good quality ice layer. Further studies were conducted and reported in [33] leading to a similar conclusion. However, these results should be generalized using a larger number of simulations and icing conditions.

Together with the icing model, the multistep algorithm leads to improvements in shape quality in an optimal amount of time. Multistep results obtained with ICECREMO2 compare reasonably well with experiments and compared well to standard ice prediction code results. The accuracy of the simulation is limited by the icing model: ice may only grow perpendicular to the airfoil surface. This is questionable, particularly in glaze ice conditions, and alternative models should be investigated.

## Acknowledgments

This research work forms part of the ICECREMO2 project. ICECREMO2 is a three-dimensional ice accretion and water flow code developed collaboratively by Airbus UK, BAe Systems, Dunlop Aerospace (Meggitt), Rolls-Royce, Westland Helicopters Ltd. (now AgustaWestland), QinetiQ, and Cranfield University under the auspices of the United Kingdom Department of Trade and Industry.

The Authors would like to thank T. G. Myers, University of Cape Town, South Africa, for his useful comments. J. P. F. Charpin acknowledges the support of the Mathematics Applications Consortium for Science and Industry funded by the Science Foundation Ireland mathematics initiative grant 06/MI/005.

## References

[1] Sparaco, P., "Swedish Crash Prompts Clear-Ice Guidelines," *Aviation Week and Space Technology*, Vol. 140, No. 2, 1994, pp. 49–50.

[2] Pereira, M., "Status of NTSB Aircraft Icing Certification-Related Safety Recommendations Issued as a Result of the 1994 ATR-72 Accident at Roselawn, IN," AIAA Paper 97-0410, 1997.

[3] Wright, W. B., "User Manual for the NASA Glenn Ice Accretion Code LEWICE," Ver. 2.2.2, NASA CR-2002-211793, 2002.

[4] Hedde, T., and Guffond, D., "ONERA 3-Dimensional Icing Model," *AIAA Journal*, Vol. 33, No. 6, 1995, pp. 1038–1045. doi:10.2514/3.12795

[5] Gent, R. W. "TRAJICE2-A Combined Water Droplet Trajectory and Ice Accretion Prediction Program for Aerofoils," Royal Aerospace Establishment TR 90054, 1990.

[6] Brahmini, M. T., Tran, P., Tezok, F., and Paraschivoiu, I., "Prediction of Ice on Supercritical and Multi-Elements Airfoils," AIAA Paper 95-0754, 1995.

[7] Eberhardt, S., and Ok, H., "Aircraft Icing Predictions Using an Efficient, Incompressible Navier–Stokes Solver," AIAA Paper 1994-609, 1996.

[8] Mingione, G., Brandi, V., and Esposito, B., "Ice Accretion Prediction on Multi-Element Airfoil," AIAA Paper 1997-0177, 1997.

[9] Bourgault, Y., Habashi, W. G., and Beaugendre, H., "Development of a Shallow Water Icing Model in FENSAP-ICE," AIAA Paper 99-0246, 1999.

[10] Messinger, B. L., "Equilibrium Temperature of an Unheated Icing Surface as a Function of Air Speed," *Journal of the Aeronautical Sciences*, Vol. 20, No. 1, 1953, pp. 29–42.

[11] Myers, T. G., "Extension to the Messinger Model for Aircraft Icing," *AIAA Journal*, Vol. 39, No. 2, 2001, pp. 211–218. doi:10.2514/2.1312

[12] Myers, T. G. and Hammond, D. W., "Ice and Water Film Growth from Incoming Supercooled Droplets," *International Journal of Heat and Mass Transfer*, Vol. 42, No. 12, 1999, pp. 2233–2242. doi:10.1016/S0017-9310(98)00237-3

[13] Myers, T. G., Charpin, J. P. F., and Chapman, S. J., "The Flow and Solidification of a Thin Fluid Film on an Arbitrary Three-Dimensional Surface," *Physics of Fluids*, Vol. 14, No. 8, 2002, pp. 2788–2803. doi:10.1063/1.1488599

[14] Gent, R. W., Dart, N. P., and Cansdale, J. T., "Aircraft Icing," *Philosophical Transactions of the Royal Society of London. Series A, Mathematical Physical and Engineering Sciences*, Vol. 358, No. 1776, 2000, pp. 2873–2911. doi:10.1098/rsta.2000.0689

[15] Kind, R. J., Potapczuk, M. G., Feo, A., Golia, C., and Shah, A. D., "Experimental and Computational Simulation of In-Flight Icing Phenomena," *Progress in Aerospace Sciences*, Vol. 34, No. 5–6, 1998, pp. 257–345. doi:10.1016/S0376-0421(98)80001-8

[16] Ruff, G. A., and Berkowitz, B. M., "Users Manual for the NASA Lewis Ice Accretion Prediction Code (LEWICE)," NASA CR-185129, 1990.

[17] Guffond, D., and Hedde, T., "Prediction of Ice Accretion: Comparison between the 2D and 3D Codes," *La Recherche Aerospatiale: Bulletin Bimestriel de l'Office National d'Etudes et de Recherches Aerospatiales*, Vol. 2, 1994, pp. 103–115.

[18] Yamaguchi, K., Hansman, R. J., and Kazmierczak, M., "Deterministic Multi-Zone Ice Accretion Modeling," AIAA Paper 1991-0265, 1991.

[19] Wright, W. B., and Rutkowski, A., "Validation Results for LEWICE 2.0," NASA CR 1999-208690, 1999.

[20] Wright, W. B. "User Manual for the NASA Glenn Ice Accretion Code LEWICE," Ver. 2.0, NASA CR 1999-209409, 1999.

[21] Wright, W. B., and Bidwell, C. S., "Additional Improvements to the NASA Lewis Ice Accretion Code LEWICE," AIAA Paper 1995-0752, 1995.

[22] Wright, W. B., Gent, R. W., and Guffond, D., "DRA/NASA/ONERA Collaboration on Icing Research: Part II—Prediction of Airfoil Ice Accretion," NASA CR 202349, 1997.

[23] Myers, T. G., Charpin, J. P. F., and Thompson, C. P., "Slowly Accreting Ice due to Supercooled Water Impacting on a Cold Surface," *Physics of Fluids*, Vol. 14, No. 1, 2002, pp. 240–256. doi:10.1063/1.1416186

[24] Myers, T. G., and Charpin, J. P. F., "A Mathematical Model for Atmospheric Ice Accretion and Water Flow on a Cold Surface," *International Journal of Heat and Mass Transfer*, Vol. 47, No. 25, 2004, pp. 5483–5500. doi:10.1016/j.ijheatmasstransfer.2004.06.037

[25] Shin, J., and Bond, T. H., "Results of an Icing Test on a NACA 0012 Airfoil in the NASA Lewis Icing Research Tunnel," AIAA Paper 92-0647, 1992.

[26] Kind, R. J. (ed.), "Ice Accretion Simulation Evaluation Test," North Atlantic Treaty Organization RTO Technical Rept. TR-038, Neuill-sur-Seine, France, 2001.

[27] Spalart, P. R., and Allmaras, S. R. "A One-Equation Turbulence Model for Aerodynamic Flows," AIAA Paper 92-0439, 1992.

[28] Chung, J. J. and Addy, H. E. "A Numerical Evaluation of Icing Effects on a Natural Laminar Flow Airfoil," AIAA Paper 2000-0096, 2000.

[29] Mingione, G., and Brandi, V., "Ice Accretion Prediction on Multi-Elements Airfoils," *Journal of Aircraft*, Vol. 35, No. 2, 1998, pp. 240–246. doi:10.2514/2.2290

[30] Wright, W. B., "Users Manual for the Improved NASA Lewis Ice Accretion Code LEWICE," Ver. 1.6, NASA CR 198355, 1995.

[31] Hedde, T., and Guffond, D., "Development of a Three-Dimensional Icing Code, Comparison with Experimental Shapes," AIAA Paper 92-0041, 1992.

[32] Hedde, T., and Guffond, D., "Improvement of the ONERA-3D Icing Code, Comparison with 3D Experimental Shapes," AIAA Paper 93-0169, 1993.

[33] Verdin, P., "An Automatic Multi-Stepping Approach for Aircraft Ice Prediction," Ph.D. Dissertation, School of Engineering, Cranfield University, Cranfield, Bedfordshire, UK, 2007.